Cryptococcus neoformans evades pulmonary immunity by modulating xylose transport

Lucy X. Li[a*], Camaron R. Hole[a], Javier Rangel-Moreno[b], Shabaana A. Khader[a], and Tamara L. Doering[a,#]

[a]Department of Molecular Microbiology, Washington University School of Medicine, St. Louis, Missouri, USA

[b]Department of Medicine, Allergy/Immunology, and Rheumatology, University of Rochester School of Medicine, Rochester, New York, USA

Running Head: Xylose and cryptococcal immunity

[#]Address correspondence to Tamara L. Doering, doering@wustl.edu.

*Present address: Department of Medicine, Johns Hopkins University School of Medicine, Baltimore, Maryland, USA

ABSTRACT

Cryptococcus neoformans is a fungal pathogen that kills almost 200,000 people each year and is distinguished by abundant and unique surface glycan structures that are rich in xylose. A mutant strain of *C. neoformans* that cannot transport xylose precursors into the secretory compartment is severely attenuated in virulence in mice, yet surprisingly is not cleared. We found that this strain failed to induce the non-protective T helper cell type 2 (Th2) responses characteristic of wild type infection, instead promoting sustained Interleukin (IL)-12p40 induction and increased IL-17A (IL-17) production. It also stimulated dendritic cells to release high levels of pro-inflammatory cytokines, a behavior we linked to xylose expression. Finally, we discovered that inducible bronchus associated lymphoid tissue (iBALT) forms in response to cryptococcal infection. Although iBALT formation is delayed upon infection with xylose-deficient cryptococci, it subsequently restricts infection. These studies demonstrate that cryptococcal infection triggers iBALT formation and elucidate the role of xylose in the modulation of host response to this fungal pathogen.

INTRODUCTION

Cryptococcus neoformans is a ubiquitous environmental fungus that causes pneumonia and meningitis. This opportunistic pathogen infects over a million individuals each year, with overall mortality exceeding 20% (1-3). Patient immune status is the main determinant of infection outcome, highlighting the importance of efficient host immune responses in the control of cryptococcosis.

C. neoformans infection begins when the organism is inhaled, followed by its proliferation in the lungs. This pulmonary infection may then disseminate to the brain, where it causes a frequently lethal meningoencephalitis. In the lungs, *C. neoformans* first interacts with host macrophages and dendritic cells (DC). These can engulf the fungus and migrate to draining lymph nodes, where they present antigen to T cells to initiate the adaptive immune response. The protective immune response to *C. neoformans* is primarily mediated by T cells. Although T helper cell type 1 (Th1) responses are protective against *C. neoformans* (4), it is likely that T helper type 17 (Th17) responses participate in pathogen clearance at mucosal surfaces (5-7). In contrast, T helper cell type 2 (Th2) responses are considered detrimental for protective immunity, leading to fungal growth and facilitating dissemination to the CNS (8, 9). The induction of these non-protective responses is not well understood, but cryptococcal glycans may contribute to this process (10).

Glycan structures participate in antigen recognition, immune activation, or immune regulation in multiple organisms (11). In *C. neoformans* the major virulence factor, a polysaccharide capsule, modulates the immune response via multiple mechanisms (12, 13). The capsule is primarily composed of two large polysaccharides: glucuronoxylomannan

(GXM) and glucuronoxylomannogalactan (GXMGal) (14, 15). One major component of both polymers is xylose (Xyl), which comprises almost one fourth of the polysaccharide capsule mass (16). Xylose also occurs in cryptococcal glycolipids (17) and as both Xyl and Xyl-phosphate modifications of protein-linked glycans (18-20). We demonstrate here that Xyl plays a critical role in the immune recognition of, and response to, *C. neoformans.*

The incorporation of Xyl into cryptococcal glycan structures occurs in the lumen of the secretory pathway, via enzymatic reactions that use the substrate molecule UDP-Xyl. This xylose donor is imported into the synthetic compartment by two transporters, Uxt1 and Uxt2 (21). A mutant strain that lacks both transporters (*uxt1*Δ *uxt2*Δ) exhibits defects in glycosylation, including incomplete synthesis of capsule polysaccharides, and considerable attenuation of virulence in mouse models of infection. Surprisingly, despite its compromised virulence, this attenuated strain persists in the lungs of infected mice. In pursuing the mechanism of this persistence, we observed the formation of inducible bronchus associated lymphoid tissue (iBALT) in the lungs of both wild-type (WT) and *uxt1*Δ *uxt2*Δ infected mice. In the lungs of mice infected with the mutant strain, iBALT formation was significantly delayed. However, once formed, it was better organized than the iBALT formed when mice were infected with fully xylosylated WT *C. neoformans.* Furthermore, animals infected with the mutant experienced a long-term asymptomatic infection rather than the rapid and lethal disease observed upon WT infection. Together, these results suggest that luminal Xyl modifications of cryptococcal glycoconjugates interfere with immune recognition and activation of immune cells, events that are required for efficient control of the pulmonary infection.

RESULTS

UDP-Xyl transport is required for cryptococcal virulence and dissemination

We previously observed that a *C. neoformans* strain lacking UDP-Xyl transporters (*uxt1*Δ *uxt2*Δ) was highly attenuated in virulence compared to the WT parental strain KN99α, yet persisted in the lungs of asymptomatic mice for at least 100 days after infection (21). To investigate the development of this chronic infection, we first examined the kinetics of fungal burden in mice after intranasal inoculation with WT and mutant strains. In A/JCr mice infected intranasally with WT fungi, which typically succumb to infection roughly 18 days post-infection (dpi), we observed a rapid and significant increase in pulmonary fungal burden (Fig 1A) along with significant dissemination to the spleen (Fig 1B) and brain (Fig 1C). In contrast, the pulmonary burden in *uxt1*Δ *uxt2*Δ-infected mice increased only gradually from initial inoculum levels to a modest peak at 63 dpi (Fig 1A). Colony-forming units in the lung then gradually declined, with complete clearance occurring in 30% of the mice by 189 dpi (Fig 1A). Although this infection was not limited to the lungs, only a fraction of the mice had measurable *uxt1*Δ *uxt2*Δ cells in the spleen (Fig 1B) and brain (Fig 1C) at 63 dpi. Furthermore, this limited dissemination was only observed at the times of highest lung burden (63 and 126 dpi), with no fungi detected at distal sites by 189 dpi (Fig 1B, Fig 1C). These results suggest that the A/JCr mice would eventually clear the *uxt1*Δ *uxt2*Δ infection.

Cryptococcal xylosylation influences differential production of pulmonary cytokines.

We next sought to identify the mechanism(s) responsible for the protracted host clearance of *uxt1*Δ *uxt2*Δ infection. As summarized above, protection against *C. neoformans* is generally associated with production of type 1 cytokines like interleukin (IL)-2, IL-12, interferon gamma (IFN-γ), and tumor necrosis factor alpha (TNF-α). In contrast, a Th2 response to cryptococcal infection (characterized by the production of IL-4, IL-5, IL-10, and IL-13) compromises control of pulmonary fungal burden (22) and facilitates dissemination to the central nervous system (4, 22).

We hypothesized that the increased survival of mice infected with the mutant cryptococci reflected an alteration in the immune response elicited by pulmonary infection. To test this hypothesis, we analyzed cytokine levels over time in lung homogenates from mice infected with WT or *uxt1*Δ *uxt2*Δ strains (Fig 1). A strong Th2-type response with significant induction of IL-4 and IL-5 over the 15 days prior to sacrifice was detected in mice infected with WT cryptococci (Fig 1D, Fig 1E). In contrast, *uxt1*Δ *uxt2*Δ cells elicited a more quiescent cytokine response at early stages of infection. Furthermore, at the peak of fungal burden in *uxt1*Δ *uxt2*Δ-infected mice (day 63, Fig. 1A), there was a significant increase in the Th1 polarizing cytokine IL-12p40 compared to the levels observed in naïve lungs (Fig 1F). Subsequently, IL-12p40 levels slowly declined, along with fungal burden (Fig 1F). Although levels of IFNγ and TNFα (Fig 1G, Fig 1H) were similar to those in the lungs of naïve mice, IL-17 trended higher at the peak of infection (Fig 1I). Overall, while WT infection rapidly induced non-protective Th2 responses, infection with *uxt1*Δ *uxt2*Δ failed to do so (even at the peak of fungal burden) and instead promoted the sustained induction of IL-12p40 and increased production of IL-17.

105

106 *Inducible bronchus-associated lymphoid tissue develops following cryptococcal infection*

107 The differences that we observed in fungal burden and cytokine levels between mutant
108 and WT infection suggested alterations in the immune response at the cellular level. To
109 test this, we performed blinded morphometric analysis of inflammatory cell infiltration in
110 the lungs at 15 dpi in mice infected with WT fungi and at 15 and 189 dpi in *uxt1*Δ *uxt2*Δ-
111 infected mice. The animals infected with the mutant strain showed significantly reduced
112 lung inflammation at both time points (Fig 2A), consistent with the more quiescent cyto-
113 kine response reported above (Fig 1). We also noted distinctive lymphocytic accumula-
114 tions proximal to the basal side of the bronchial epithelium in both groups of mice (Fig
115 2B). The lymphoid populations within these structures were organized into B cell follicles
116 surrounded by $CD3^+$ T cell cuffs (Fig 2C). The cellular composition of these inflammatory
117 foci suggested inducible bronchus-associated lymphoid tissue (iBALT) (23).

118

119 iBALT is a tertiary lymphoid tissue that forms in the lung. It resembles secondary lymphoid
120 organs (lymph nodes) in cellular composition and organization, with two distinctive zones:
121 the B cell follicle and the T cell zone (24). The B cell follicle contains mainly follicular B
122 cells and its organization is maintained by the continuous production of CXCL13. It is
123 surrounded by a T cell zone that contains CD4 and CD8 T cells as well as dendritic cells
124 (DCs) (25). At 15 dpi with WT cryptococci, we observed numerous iBALT structures, with
125 compact B cell follicles surrounded by T cells (Fig 2C, Fig 2D). In contrast, we found
126 considerably fewer and less organized B cell follicles at 15 dpi in mice infected with the
127 *uxt1*Δ *uxt2*Δ strain (Fig 2C, Fig 2D). By late in infection (189 dpi for *uxt1*Δ *uxt2*Δ and 15

dpi for WT), although iBALT structures in mice infected with the mutant strain were still less abundant than those found in lungs of WT (Fig. 2D), their average size was significantly larger (Fig. 2E). Additionally, the iBALT was more organized and even contained IgG^+ plasma cells (Fig 2C). Early in *uxt1*Δ *uxt2*Δ infection, the compromised formation of iBALT structures was accompanied by increased peri-vascular accumulation of T cells (Fig. 2F) and a significantly decreased production of CXCL13 (Fig 2G, Fig2H), a chemokine essential for iBALT formation and organization (23). In contrast, at late time points in this protracted developmental process, T cell cuffing was significantly reduced (Fig 2F) and CXCL13 expression was increased (Fig 2G, Fig 1H). While infection with WT cryptococci induced early and robust formation of iBALT, *uxt1*Δ *uxt2*Δ infection induced delayed but ultimately larger iBALT.

To quantify the host adaptive immune response to *uxt1*Δ *uxt2*Δ, we used flow cytometry to enumerate lymphocytes in the lungs of mice infected with WT or *uxt1*Δ *uxt2*Δ cells. By 12-15 dpi, the fraction of $CD19^+$ B cells (Fig 3A) or T cells ($CD4^+$ and $CD8^+$; Fig 3B, Fig 3C) in *uxt1*Δ *uxt2*Δ-infected mice significantly exceeded those of WT-infected mice, and continued to accumulate as infection progressed. The total numbers of cells in these populations remained elevated through 126 dpi (Fig. 3A-C, right), although they subsequently declined, consistent with the decreased average size in T cell cuffing observed at 189 versus 15 dpi (Fig 2F).

Survival of uxt1Δ uxt2Δ-infected mice is dependent on T cells

To test the protective role of T and B cells in the prolonged survival of *uxt1*Δ *uxt2*Δ-infected mice, we examined whether ablation of these cell types altered the course of infection. Because the mouse strains used for these studies were engineered in the C57BL/6 background, we included infections of this strain as controls. C57BL/6 mice are less resistant to *C. neoformans* than A/JCr mice used above (26), as shown by their eventual susceptibility to *uxt1*Δ *uxt2*Δ infection (Fig. 3D, solid black line). In contrast, *Rag1*-/- mice were significantly more susceptible to this strain, and succumbed by 55 dpi (Fig 3D; solid blue line).

Since *Rag1*-/- mice lack both T and B cells, we also infected mice deficient in either T cells (*TCRβ* -/-) or B cells (*μMT*) with *uxt1*Δ *uxt2*Δ cryptococci. B cell deficient mice exhibited a more protracted course of disease than *Rag1*-/-, succumbing over an 85-day period (Fig 3D, solid green line), while mice lacking only T cells succumbed to infection with kinetics similar to those of the *Rag1*-/- mice (Fig 3D, solid red line). In contrast, all mice inoculated with WT *C. neoformans* succumbed by 20 dpi (Fig 3D; dashed lines). Of this group, *Rag1*-/- and *TCRβ*-/- mice still succumbed slightly faster than C57BL/6 and μMT mice (Fig 3D). Together, these data show that T cells are the prominent cell type responsible for increased survival of *uxt1*Δ *uxt2*Δ-infected mice, although B cells may also play a role in protection.

Lack of luminal xylose modification in C. neoformans stimulates DC activation

DCs are critical for induction of protective immunity against *C. neoformans* (27), and their activation and cytokine production are required for iBALT formation and maintenance (25,

28). During iBALT formation, antigen-driven activation of DCs and their consequent cytokine and chemokine production are likely responsible for T and B cell recruitment (25), which could potentially both induce the observed increase in these cell populations and contribute to the protective effect of T cells during cryptococcal infection. For these reasons, we wished to specifically measure DC responses. To do this we tested DC interactions with WT cryptococcal cells, which exhibit antigens modified with Xyl, and *uxt1*Δ *uxt2*Δ cryptococci, which are impaired in these modifications. We also tested single *uxt*Δ mutants: *uxt1*Δ shows an intermediate level of Xyl utilization while *uxt2*Δ is similar to WT (21). In these assays, we measured the ability of heat-killed fungi to stimulate the production of pro-inflammatory cytokines by DC, comparing WT, *uxt1*Δ *uxt2*Δ, single *uxt* mutants, *uxs1*Δ (which lacks all Xyl modification because it cannot synthesize UDP-Xyl), and an acapsular control strain (*cap59*Δ) that induces a potent DC response (29). We found that bone marrow derived DCs (BMDCs) cultured with *uxt1*Δ *uxt2*Δ cells released high levels of IL-1β, IL-6, and TNF-α, similar to the levels observed following exposure to a completely acapsular control strain, *cap59*Δ (Fig 4A-C). In contrast, individual *uxt* mutants and *uxs1*Δ induced IL-1β and IL-6 levels similar to those induced by WT fungi (close to background levels; Fig 4A, Fig 4B). TNF-α similarly showed the greatest response upon challenge with *uxt1*Δ *uxt2*Δ, with levels like those induced by an acapsular strain, although some increase was also noted with other xylose-deficient strains (*uxt1*Δ and *uxs1*Δ). These results suggest that early interaction with DCs and consequent induction of proinflammatory cytokines are regulated by Xyl expression in Cryptococcus.

DISCUSSION

196 In this study, we report for the first time that *C. neoformans* infection triggers iBALT for-
197 mation. Notably, the iBALT detected in our experimental infections resembles subpleural
198 nodules that have been observed in cryptococcosis patients (30). To our knowledge, the
199 only other fungus reported to induce iBALT is *Pneumocystis* (31). Further examination
200 will be necessary to establish the similarities between histological features of inflamma-
201 tory cell infiltration in mice and humans infected with *C. neoformans* and to delineate the
202 molecular host-pathogen interactions that drive iBALT formation following *C. neoformans*
203 infection.
204
205 When we infected mice with mutant fungi unable to use Xyl for luminal glycoconjugate
206 synthesis (*uxt1*Δ *uxt2*Δ), we observed a delay in fungal accumulation and in the organi-
207 zation of the iBALT structures. When *uxt1*Δ *uxt2*Δ burden did peak, it was accompanied
208 by a rise in IL-12p40 (Fig 1F), a cytokine normally required for inducing a protective re-
209 sponse against *C. neoformans* (32), which may have facilitated subsequent resolution
210 of the *uxt1*Δ *uxt2*Δ infection. A change in IL-12p40 level might reflect an increase in ei-
211 ther IL-23 or IL-12 (33), which stimulate a Th17 or Th1 type response, respectively; the
212 former is required for iBALT formation(31). Since we saw no difference in IFN-γ levels,
213 IL-12p40 is more likely associated with a Th17 response. We did observe a trend to-
214 wards increased IL-17 levels when *uxt1*Δ *uxt2*Δ burden was the highest, which was ab-
215 sent in WT infection. Our results show that cryptococcal infection can induce iBALT
216 structures, although this does not prevent mice from succumbing to the disease. We fur-
217 ther show that the kinetics of iBALT formation and its organization are dependent on vir-
218 ulence factors of the pathogen. Future studies should futher define the functional role of

iBALT in mediating immunity to Cryptococcus and determine whether the iBALT is mediating early and local immune protection in the lung.

DCs reacted more strongly to *uxt1*Δ *uxt2*Δ than to WT *in vitro*, releasing greater amounts of pro-inflammatory cytokines (Fig 4A-C), even though the global cytokine response to the mutant is less perturbed (Fig 1D-I). These cytokines may directly or indirectly lead to the increased recruitment of T and B cells in *uxt1*Δ *uxt2*Δ infection (Fig 3A-C) and perhaps accelerate compartmentalization into compact B cell follicles and discrete T cell areas in iBALT (Fig 2). Such differences in cellular composition and organization, coupled with the differences in the local cytokine production, may confer distinct properties on the iBALT induced by WT and *uxt1*Δ *uxt2*Δ, influencing their ability to protect against *C. neoformans*.

We expected that the highly immunostimulatory behavior of *uxt1*Δ *uxt2*Δ *in vitro* reflected the lack of Xyl modifications on its surface glycoconjugates, a consequence of the absence of UDP-Xyl transport into the secretory compartment. We were surprised, therefore, that mutants unable to synthesize UDP-Xyl (*uxs1*Δ), which similarly lack Xyl modifications on secreted glycoconjugates, did not phenocopy this broad and robust DC response. This suggests that Uxs1 itself is required for the strong response seen in the absence of xylosylation in the secretory pathway. It may be that this protein plays additional roles unrelated to glycosylation, or that the stimulatory component is dependent on cytosolic UDP-Xyl, rather than UDP-Xyl that has been transported into the secretory pathway.

242 Unlike encapsulated strains, *C. neoformans* mutants lacking capsule induce the upregu-
243 lation of multiple genes involved in cytokine responses and enhance antigen processing
244 and presentation by DCs (34). Interestingly, the cytokine levels induced in DC by the
245 *uxt1*Δ *uxt2*Δ mutant were similar to those induced by the acapsular mutant *cap59*Δ (Fig
246 4A-C). Xyl may thus be critical for the immune suppressive effects normally exerted by
247 capsule material. The mechanisms behind the robust DC activation seen in these two
248 mutants, including the cellular receptors and fungal components responsible, remain to
249 be determined. It is possible that the *uxt1*Δ *uxt2*Δ mutant lacks immune suppressive
250 mechanisms that are present in WT *C. neoformans* infection, and therefore induces ro-
251 bust cytokine responses and consequent recruitment of T and B cells to limit early infec-
252 tion. Further studies addressing the nature, type, and extent of the T and B cell responses
253 in the context of WT and *uxt1*Δ *uxt2*Δ infection should allow us to fully understand the the
254 initiation, formation, and organization of iBALT structures in the lung during *C. neofor-*
255 *mans* infection. Further, as iBALT is induced in WT *C. neoformans* infection where the
256 mice succumb to the disease, it is unclear if iBALT structures play a protective or patho-
257 logical role in immunity. Specific chemokine deficient mice, such as CXCL-13 deficient
258 animals that lack the ability to induce iBALT structures (35), will be useful in future studies
259 to define the function of iBALT in fungal infections.
260
261 Control of *uxt1*Δ *uxt2*Δ infection requires both T and B cells (Fig 3D), which suggests that
262 iBALT formation may play a key role in restricting disease. Even in the absence of T and

263 B cells, however, mutant-infected mice still survived more than twice as long as WT-in-
264 fected animals (Fig 3D). This may be due to the slightly slower growth of the mutant,
265 which we have previously observed (21).
266
267 We have found that *C. neoformans* infection induces iBALT formation, although the for-
268 mation of iBALT by itself is insufficient to protect against wild-type fungal infection. Inoc-
269 ulation with a *uxt1*Δ *uxt2*Δ strain, however, induced similar lymphoid structures, which do
270 appear to restrict infection despite their delayed organization. *In vitro*, this mutant induced
271 DCs to release much higher levels of proinflammatory cytokines than WT fungi. This is
272 presumably a consequence of the lack of surface Xyl modification, suggesting a role for
273 this structure in the immunosuppressive features of capsule polysaccharides or other sur-
274 face exposed or secreted glycoconjugates, although the full mechanism remains to be
275 defined. By influencing the dynamics of the inflammatory process, we may be able to
276 improve pulmonary responses to help control infection and use this information to help
277 guide novel therapies that stimulate the induction of protective lung fungal immunity.
278
279 **MATERIALS AND METHODS**
280 *Fungal strains*
281 *C. neoformans* strains (Table S1) were grown at 30 °C in YPD medium (1% [wt/vol] yeast
282 extract, 2% [wt/vol] peptone, 2% [wt/vol] dextrose) with shaking (230 rpm) or on YPD agar
283 plates (YPD medium with 2% [wt/vol] agar) supplemented with the following antibiotics as
284 appropriate: 100 μg/ml nourseothricin (NAT; Werner BioAgents) or Geneticin (G418; Invi-
285 trogen).

286

287 *Mice*

288 C57BL/6J (RRID: IMSR_JAX:000664) and A/JCr (RRID: IMSR_CRL:563) mice were ob-
289 tained from Jackson Laboratory. *Rag1*-/- (RRID: IMSR_JAX:002216), *TCRβ*-/- (RRID:
290 IMSR_JAX:002118), and μMT mice (RRID: IMSR_JAX:002288) (all on C57BL/6 back-
291 ground) were generously provided by Dr. Michael Diamond and Dr. Wayne Yokoyama
292 (Washington University School of Medicine); breeders were originally purchased from
293 Jackson Laboratory. All mice were 6 to 8 weeks old at the time of infection. A/JCr mice
294 were female; male and female mice were used for the other strains with gender and age
295 matched C57BL/6 controls.

296

297 *Ethics statement*

298 All animal protocols were reviewed and approved by the Animal Studies Committee of
299 the Washington University School of Medicine and conducted according to National Insti-
300 tutes of Health guidelines for housing and care of laboratory animals.

301

302 *C. neoformans infection*

303 Fungal strains were cultured overnight (O/N) and diluted to 10^6 cells/mL in sterile PBS.
304 Mice were intranasally inoculated with a 50 μL aliquot, and then weighed and monitored
305 daily. Infected mice were sacrificed if they lost >20% relative to peak weight or at specified
306 time points. At the time of sacrifice, mice were perfused intracardially with 10 mL sterile
307 PBS, and organs were processed as described below for fungal burden, histology, flow
308 cytometric analysis, and cytokine measurements.

Organ burden and cytokines

Brain and spleen homogenates were harvested and plated for CFU at the specified time points. 50 µL aliquots of the left lung homogenates (V_T = 1 mL) were similarly plated for CFUs. The remaining sample was assayed for pulmonary cytokine levels using the Bio-Plex Protein Array System (Bio-Rad Laboratories). Briefly, the lung homogenates were mixed with an equal volume of PBS/0.1% Triton 100x/2x protease inhibitor (Pierce EDTA-free protease inhibitor; Thermo Scientific), vortexed for 3 seconds, and clarified by centrifugation (2500 x g, 10 min). Supernatant fractions were then assayed using the Bio-Plex Pro Mouse Cytokine 23-Plex (Bio-Rad Laboratories) for the presence of IL-1α, IL-1β, IL-2, IL-3, IL-4, IL-5, IL-6, IL-9, IL-10, IL-12 (p40), IL-12 (p70), IL-13, IL-17A, granulocyte colony stimulating factor (G-CSF), granulocyte monocyte colony stimulating factor (GM-CSF), interferon-γ (IFN-γ), CXCL1/keratinocyte-derived chemokine (KC), CCL2/monocyte chemotactic protein-1 (MCP-1), CCL3/macrophage inflammatory protein-1α (MIP-1α), CCL4/MIP-1β, CCL5/regulated upon activation normal T cell expressed and secreted (RANTES), and tumor necrosis factor-α (TNF-α).

Immunofluorescence staining and histologic analysis

Mice were perfused intracardially with sterile PBS, and the lungs inflated with 10% formalin. Lung tissue was then fixed O/N in 10% formalin, and submitted to the Washington University Developmental Biology Histology Core for paraffin-embedding, sectioning, and staining with H & E. Immunofluorescence staining for B cells (APC-conjugated rat anti-mouse CD45R/B220, clone RA3-6B2, BD Biosciences, RRID: AB_627078), T cell cuffing

(CD3-ε, clone M-20, Santa Cruz Biotechnology, RRID: AB_631129), and CXCL13-producing cells (goat α-mouse CXCL13, AF470, R&D Systems, RRID: AB_355378) was performed as in Ref (31). Images were taken with a Zeiss Axioplan2 microscope and recorded with a Hamamatsu camera. Blinded morphometric analysis of lung structures was performed with the outline tool of Zeiss Axiovision software.

Flow cytometric analysis

The right lung of individual mice was enzymatically digested (in 5 mL RPMI with 1 mg/mL collagenase type IV) at 37 °C with shaking (230 rpm) for 30 min, and then sequentially passed through sterile 70 and 40 µm pore nylon strainers (BD Biosciences, San Jose, CA). Red blood cells in the samples were lysed by treatment for 3 min on ice with 5 mL ammonium-chloride-potassium lysing buffer (8.024 g/L NH_4Cl, 1.001 g/L $KHCO_3$, 2.722 mg/L EDTA•Na_2 $2H_2O$), followed by the addition of 2 volumes of PBS. The remaining cells were pelleted (1000 x g, 5 min, 4 °C), washed twice with PBS, diluted to 10^6 cells/mL in PBS, and stained with LIVE/DEAD fixable blue dead cell stain (1:1000; Thermo Scientific). Following incubation in the dark for 30 min at 4 °C, cells were washed with PBS and FACS buffer (2% fetal bovine serum in PBS) before resuspension in FACS buffer. Samples were then blocked with CD16/CD32 (1:500; Fc Block™; BD Biosciences, RRID: AB_394656) for 5 min and incubated for 30 min with optimal concentrations of fluorochrome-conjugated antibodies (Table S2) diluted in Brilliant Stain Buffer (BD Biosciences). After three washes with FACS buffer, the cells were fixed in 2% formaldehyde/FACS buffer. For data acquisition, >50,000 events were collected on a BD LSRFortessa X-20 flow cytometer (BD Biosciences), and the data were analyzed with FlowJo

V10 (Fig. S1; TreeStar). The absolute number of cells in each leukocyte subset was determined by multiplying the absolute number of $CD45^+$ cells by the percentage of cells stained by fluorochrome-labeled antibodies for each cell population analyzed.

Isolation of bone marrow derived cells

Bone marrow was flushed from the femurs and tibiae of C57BL/6 mice using RPMI. Cells were collected (1000 x g, 5 min, 4°C), resuspended in RPMI, and counted using a hemocytometer. To prepare bone marrow derived dendritic cells (BMDCs), 2 x 10^6 bone marrow cells were plated in 10 mL R10 medium (10% FBS, 0.4% Penicillin-Streptomycin, 2 mM L-glutamate, 50 μM 2-β-mercaptoethanol in RPMI) supplemented with 1 ng/mL GM-CSF, and incubated at 37 °C and 5% CO_2. Medium was changed 3 and 6 days after plating, and cells were harvested on day 8. BMDCs were enriched by depletion of BMMs using biotinylated α-F4/80 antibody (eBioscience, RRID: AB_466657) and anti-biotin conjugated magnetic beads (Miltenyi Biotec). The BMDCs in the flow through were positively selected using α-CD11c magnetic beads according to the manufacturer's protocol (Miltenyi Biotec).

Dendritic cell assays

To assay the ability of fungal strains to activate BMDCs, *C. neoformans* strains of interest were grown O/N, washed in PBS, and incubated at 65 °C for 15 min to heat kill (HK) the fungi. BMDCs and HK fungi (10^6 cells of each) were then co-incubated for 24 h, sedimented, and the supernatant fractions transferred to 1.5 mL centrifuge tubes containing

377 10 µL of 100x protease inhibitor (ThermoScientific). IL-1β, IL-6, and TNF-α levels in su-
378 pernatants were determined by ELISA according to the manufacturer's protocol (R&D
379 systems).
380
381 *Statistical analysis*
382 Each experiment was performed a minimum of two times. Statistical analyses were con-
383 ducted using GraphPad Prism version 6.0f (GraphPad Software). All studies comparing
384 two groups were analyzed with a Student's t-test. Those with three or more groups were
385 compared using an ordinary one-way ANOVA with Tukey's *post-hoc* test. $p < 0.05$ was
386 considered statistically significant.
387
388 **ACKNOWLEDGEMENTS**
389 We thank members of the Doering laboratory for helpful discussions and assistance with
390 experiments. We also thank Dr. Thomas R. Kozel (University of Nevada School of Medi-
391 cine) for the anti-GXM monoclonal antibody, and Dr. Michael Diamond and Dr. Wayne
392 Yokoyama for immune deficient mouse lines.
393
394 This work was funded by National Institutes of Health grants R21 AI109623 and R01
395 AI102882 to TLD. LXL was partly supported by a National Research Science Award (T32
396 GM007200), a Sondra Schlesinger Graduate Fellowship (Washington University St. Louis
397 Microbiology Department), and a National Institute of Allergy and Infectious Diseases fel-
398 lowship (F30 AI120339). CRH was partly funded by a National Institute of Allergy and
399 Infectious Diseases training grant (T32 AI007172). SAK and JRM were supported by NIH

grant R01 AI111914. The funders had no role in study design, data collection and interpretation, or the decision to submit the work for publication.

AUTHOR CONTRIBUTIONS

Conceptualization, LXL, CRH, SAK, and TLD; Methodology, LXL, CRH, JRM, SAK, TLD; Investigation, LXL, CRH, and JRM; Writing – Original Draft, LXL and CRH; Writing – Review & Editing, LXL, CRH, JRM, SAK, and TLD; Funding Acquisition, LXL, SAK and TLD; Resources, SAK and TLD; Supervision, SAK and TLD.

DECLARATION OF INTERESTS

LXL, CRH, JRM, SAK and TLD have no interests to declare.

413 **References**

414

415 1. Kwon-Chung KJ, Fraser JA, Doering TL, Wang Z, Janbon G, Idnurm A, Bahn YS.
416 2014. *Cryptococcus neoformans* and *Cryptococcus gattii,* the etiologic agents of
417 cryptococcosis. Cold Spring Harb Perspect Med 4:a019760.
418 2. Denning DW. 2016. Minimizing fungal disease deaths will allow the UNAIDS target
419 of reducing annual AIDS deaths below 500 000 by 2020 to be realized. Philos
420 Trans R Soc Lond B Biol Sci 371.
421 3. Rajasingham R, Smith RM, Park BJ, Jarvis JN, Govender NP, Chiller TM, Denning
422 DW, Loyse A, Boulware DR. 2017. Global burden of disease of HIV-associated
423 cryptococcal meningitis: an updated analysis. Lancet Infect Dis
424 doi:10.1016/S1473-3099(17)30243-8.
425 4. Wozniak KL, Levitz SM. 2011. T cell and dendritic cell immune responses to
426 Cryptococcus, p p 387-396. *In* Heitman J, Kozel TR, Kwon-Chung KJ, Perfect JR,
427 Casadeval A (ed), Cryptococcus. ASM Press, Washington, DC.
428 5. Zhang Y, Wang F, Tompkins KC, McNamara A, Jain AV, Moore BB, Toews GB,
429 Huffnagle GB, Olszewski MA. 2009. Robust Th1 and Th17 immunity supports
430 pulmonary clearance but cannot prevent systemic dissemination of highly virulent
431 *Cryptococcus neoformans* H99. Am J Pathol 175:2489-500.
432 6. Wozniak KL, Hardison SE, Kolls JK, Wormley FL. 2011. Role of IL-17A on
433 resolution of pulmonary *C. neoformans* infection. PLoS One 6:e17204.
434 7. Murdock BJ, Huffnagle GB, Olszewski MA, Osterholzer JJ. 2014. Interleukin-17A
435 enhances host defense against cryptococcal lung infection through effects

436 mediated by leukocyte recruitment, activation, and gamma interferon production.
437 Infect Immun 82:937-48.
438 8. Schulze B, Piehler D, Eschke M, von Buttlar H, Kohler G, Sparwasser T, Alber G.
439 2014. CD4(+) FoxP3(+) regulatory T cells suppress fatal T helper 2 cell immunity
440 during pulmonary fungal infection. Eur J Immunol 44:3596-604.
441 9. Wiesner DL, Smith KD, Kotov DI, Nielsen JN, Bohjanen PR, Nielsen K. 2016.
442 Regulatory T cell induction and retention in the lungs drives suppression of
443 detrimental type 2 Th cells during pulmonary cryptococcal infection. J Immunol
444 196:365-74.
445 10. Wiesner DL, Specht CA, Lee CK, Smith KD, Mukaremera L, Lee ST, Lee CG, Elias
446 JA, Nielsen JN, Boulware DR, Bohjanen PR, Jenkins MK, Levitz SM, Nielsen K.
447 2015. Chitin recognition via chitotriosidase promotes pathologic type-2 helper T
448 cell responses to cryptococcal infection. PLoS Pathog 11:e1004701.
449 11. Wolfert MA, Boons GJ. 2013. Adaptive immune activation: glycosylation does
450 matter. Nat Chem Biol 9:776-84.
451 12. Zaragoza O, Rodrigues ML, De Jesus M, Frases S, Dadachova E, Casadevall A.
452 2009. The capsule of the fungal pathogen *Cryptococcus neoformans*. Adv Appl
453 Microbiol 68:133-216.
454 13. Yauch LE, Lam JS, Levitz SM. 2006. Direct inhibition of T-cell responses by the
455 Cryptococcus capsular polysaccharide glucuronoxylomannan. PLoS Pathog
456 2:e120.
457 14. Agustinho DP, Miller LC, Li LX, Doering TL. 2018. Peeling the onion: the outer
458 layers of *Cryptococcus neoformans*. Mem Inst Oswaldo Cruz 113:e180040.

15. Wang ZA, Li LX, Doering TL. 2018. Unraveling synthesis of the cryptococcal cell wall and capsule. Glycobiology 28:719-730.

16. Cherniak R, Valafar H, Morris LC, Valafar F. 1998. *Cryptococcus neoformans* chemotyping by quantitative analysis of 1H nuclear magnetic resonance spectra of glucuronoxylomannans with a computer-simulated artificial neural network. Clin Diagn Lab Immunol 5:146-59.

17. Castle SA, Owuor EA, Thompson SH, Garnsey MR, Klutts JS, Doering TL, Levery SB. 2008. Beta1,2-xylosyltransferase Cxt1p is solely responsible for xylose incorporation into *Cryptococcus neoformans* glycosphingolipids. Eukaryot Cell 7:1611-5.

18. Klutts JS, Levery SB, Doering TL. 2007. A beta-1,2-xylosyltransferase from *Cryptococcus neoformans* defines a new family of glycosyltransferases. J Biol Chem 282:17890-9.

19. Park JN, Lee DJ, Kwon O, Oh DB, Bahn YS, Kang HA. 2012. Unraveling unique structure and biosynthesis pathway of N-linked glycans in human fungal pathogen *Cryptococcus neoformans* by glycomics analysis. J Biol Chem 287:19501-15.

20. Lee DJ, Bahn YS, Kim HJ, Chung SY, Kang HA. 2015. Unraveling the novel structure and biosynthetic pathway of O-linked glycans in the Golgi apparatus of the human pathogenic yeast *Cryptococcus neoformans*. J Biol Chem 290:1861-73.

21. Li LX, Rautengarten C, Heazlewood JL, Doering TL. 2018. Xylose donor transport is critical for fungal virulence. PLoS Pathog 14:e1006765.

481 22. Koguchi Y, Kawakami K. 2002. Cryptococcal infection and Th1-Th2 cytokine
482 balance. Int Rev Immunol 21:423-38.
483 23. Moyron-Quiroz JE, Rangel-Moreno J, Kusser K, Hartson L, Sprague F, Goodrich
484 S, Woodland DL, Lund FE, Randall TD. 2004. Role of inducible bronchus
485 associated lymphoid tissue (iBALT) in respiratory immunity. Nat Med 10:927-34.
486 24. Randall TD, Carragher DM, Rangel-Moreno J. 2008. Development of secondary
487 lymphoid organs. Annu Rev Immunol 26:627-50.
488 25. Hwang JY, Randall TD, Silva-Sanchez A. 2016. Inducible bronchus-associated
489 lymphoid tissue: taming inflammation in the lung. Front Immunol 7:258.
490 26. Huffnagle GB, Boyd MB, Street NE, Lipscomb MF. 1998. IL-5 is required for
491 eosinophil recruitment, crystal deposition, and mononuclear cell recruitment during
492 a pulmonary *Cryptococcus neoformans* infection in genetically susceptible mice
493 (C57BL/6). J Immunol 160:2393-400.
494 27. Leopold Wager CM, Hole CR, Wozniak KL, Wormley FL, Jr. 2016. Cryptococcus
495 and Phagocytes: Complex Interactions that Influence Disease Outcome. Front
496 Microbiol 7:105.
497 28. Geurts van Kessel CH, Willart MA, Bergen IM, van Rijt LS, Muskens F, Elewaut D,
498 Osterhaus AD, Hendriks R, Rimmelzwaan GF, Lambrecht BN. 2009. Dendritic
499 cells are crucial for maintenance of tertiary lymphoid structures in the lung of
500 influenza virus-infected mice. J Exp Med 206:2339-49.
501 29. Grijpstra J, Tefsen B, van Die I, de Cock H. 2009. The *Cryptococcus neoformans*
502 *cap10* and *cap59* mutant strains, affected in glucuronoxylomannan synthesis,

503 differentially activate human dendritic cells. FEMS Immunol Med Microbiol 57:142-
504 50.
505 30. Haugen RK, Baker RD. 1954. The pulmonary lesions in cryptococcosis with
506 special reference to subpleural nodules. Am J Clin Pathol 24:1381-90.
507 31. Eddens T, Elsegeiny W, Garcia-Hernadez ML, Castillo P, Trevejo-Nunez G,
508 Serody K, Campfield BT, Khader SA, Chen K, Rangel-Moreno J, Kolls JK. 2017.
509 Pneumocystis-driven inducible bronchus-associated lymphoid tissue formation
510 requires Th2 and Th17 immunity. Cell Rep 18:3078-3090.
511 32. Decken K, Kohler G, Palmer-Lehmann K, Wunderlin A, Mattner F, Magram J,
512 Gately MK, Alber G. 1998. Interleukin-12 is essential for a protective Th1 response
513 in mice infected with *Cryptococcus neoformans*. Infect Immun 66:4994-5000.
514 33. Oppmann B, Lesley R, Blom B, Timans JC, Xu Y, Hunte B, Vega F, Yu N, Wang
515 J, Singh K, Zonin F, Vaisberg E, Churakova T, Liu M, Gorman D, Wagner J,
516 Zurawski S, Liu Y, Abrams JS, Moore KW, Rennick D, de Waal-Malefyt R, Hannum
517 C, Bazan JF, Kastelein RA. 2000. Novel p19 protein engages IL-12p40 to form a
518 cytokine, IL-23, with biological activities similar as well as distinct from IL-12.
519 Immunity 13:715-25.
520 34. Lupo P, Chang YC, Kelsall BL, Farber JM, Pietrella D, Vecchiarelli A, Leon F,
521 Kwon-Chung KJ. 2008. The presence of capsule in *Cryptococcus neoformans*
522 influences the gene expression profile in dendritic cells during interaction with the
523 fungus. Infect Immun 76:1581-9.
524 35. Slight SR, Rangel-Moreno J, Gopal R, Lin Y, Fallert Junecko BA, Mehra S, Selman
525 M, Becerril-Villanueva E, Baquera-Heredia J, Pavon L, Kaushal D, Reinhart TA,

526 Randall TD, Khader SA. 2013. CXCR5(+) T helper cells mediate protective
527 immunity against tuberculosis. J Clin Invest 123:712-26.

528

FIGURES WITH LEGENDS

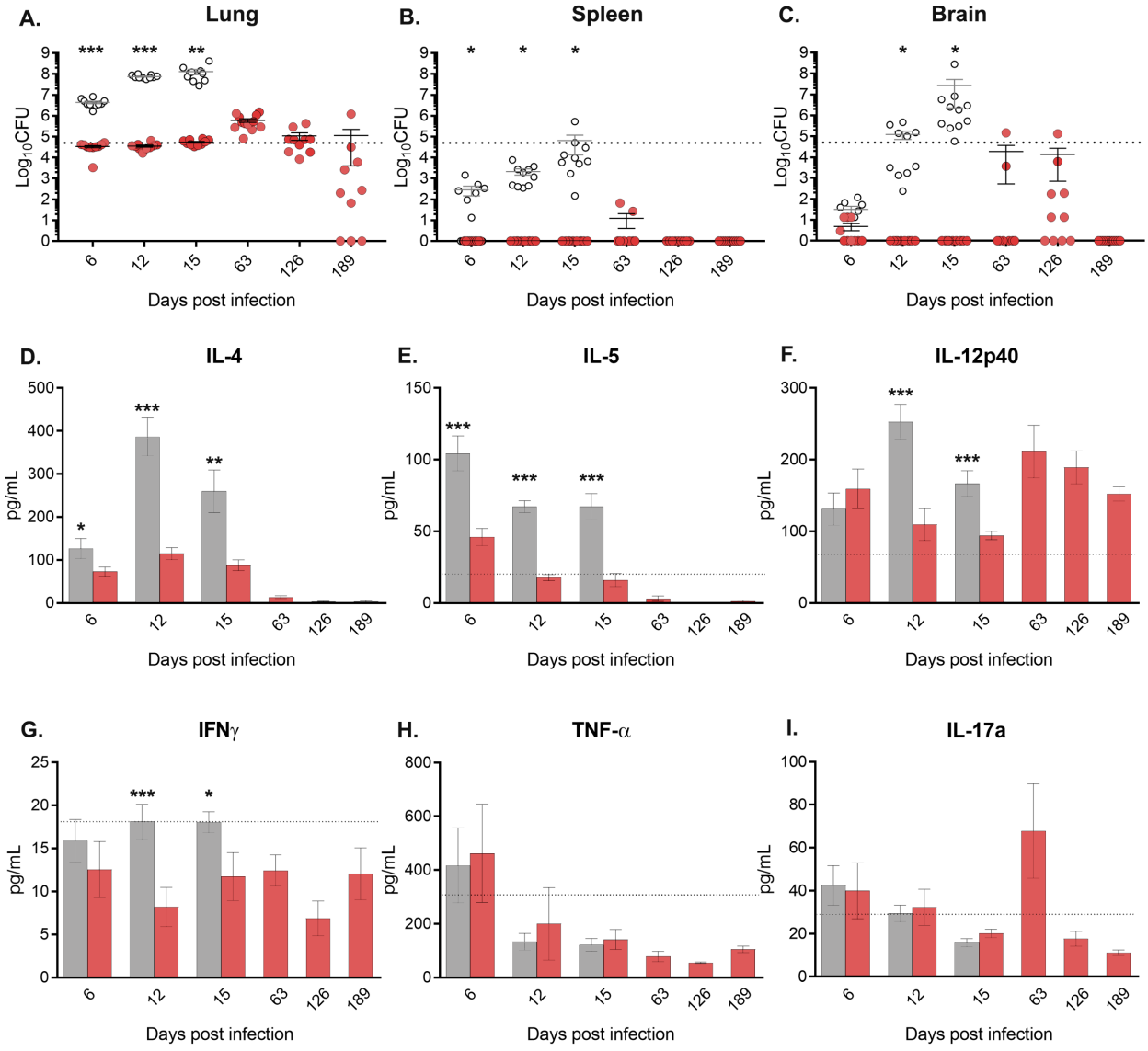

Figure 1. Fungal burden and pulmonary cytokine production in WT and *uxt1*Δ *uxt2*Δ mice. All panels show the combined results of two independent experiments (5 mice per group per experiment). (A-C) Tissue homogenates of infected A/JCr mice were plated for CFUs at the indicated dpi (open circles, WT; red circles, *uxt1*Δ *uxt2*Δ; dashed line, initial inoculum). Values from individual mice are plotted along with the mean ± SEM. (D-I) Levels of the cytokines indicated in lung homogenates over time after infection (gray bars, WT; red bars, *uxt1*Δ *uxt2*Δ; dashed line, naïve). *, $p < 0.05$; **, $p < 0.01$; ***, $p < 0.005$ for Student's t-test comparing wild type to mutant.

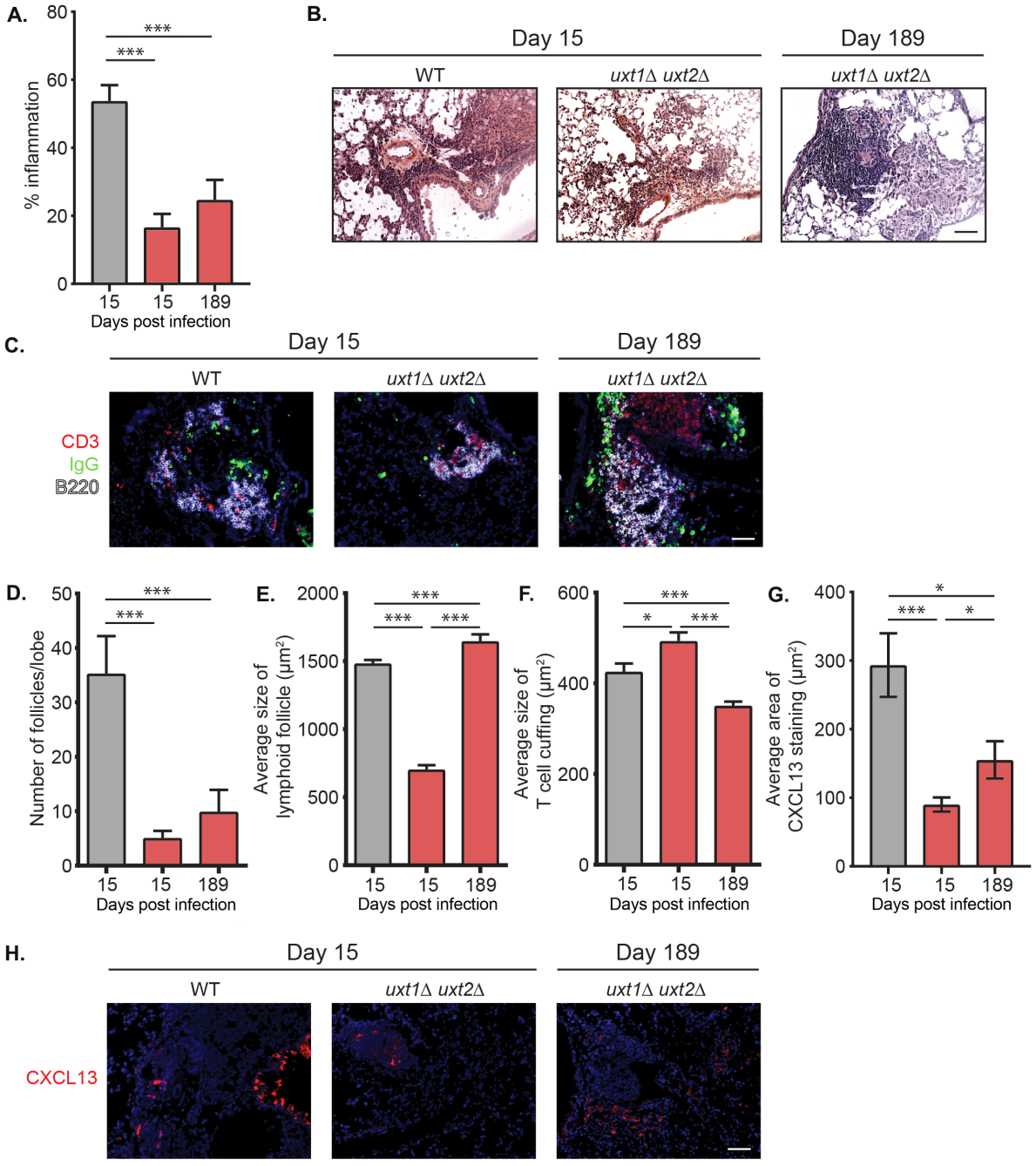

Figure 2. Inflammation and iBALT complexity in the context of *C. neoformans* infection. (A) Percent of area covered by inflammatory cells in individual lungs and (B) representative H&E micrographs from lungs collected at 15 and 189 dpi are shown. Scale bar = 100 μm. (C) Representative immunofluorescent staining of B cells ($B220^+$), T cells ($CD3^+$), and plasma cells (IgG^+) in the lungs of infected A/JCr mice. Scale bar = 100 μm. (D-F) Morphometric analysis of iBALT structures in A/JCr mice infected with WT and *uxt1*Δ *uxt2*Δ. (G,H) Quantification and examples of immunofluorescent staining of CXCL13 (red). Nuclei are stained with DAPI (blue) and scale bar = 100 μm. Plots show the combined mean ± SEM of two independent studies (4-5 mice per group per experiment). *, $p < 0.05$; ***, $p < 0.005$ by Student's t-test.

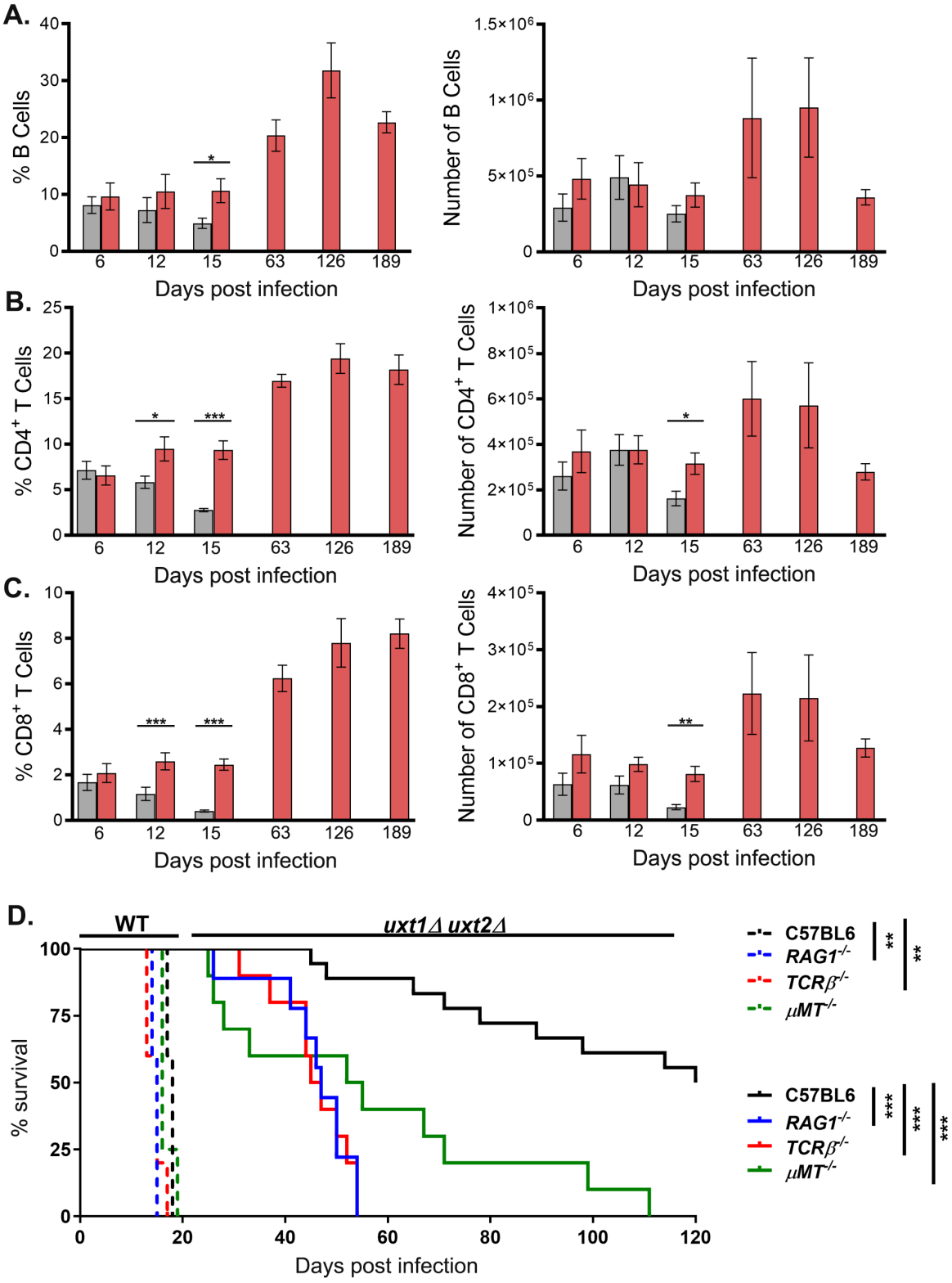

Figure 3. Accumulation of T and B cells in the lungs of mice infected with *uxt1*Δ *uxt2*Δ cells is required to prevent disease progression. (A) CD19$^+$ B cells, (B) CD4$^+$ T cells, and (C) CD8$^+$ T cells were enumerated in the lungs of infected mice by flow cytometry (gray, WT; red, *uxt1*Δ *uxt2*Δ). Plotted are the combined mean ± SEM values from two independent experiments (5

mice per group per experiment). *, $p < 0.05$; **, $p < 0.01$; ***, $p < 0.005$ by Student's t-test. (D) Survival of mice after intranasal inoculation with 5×10^4 cells of WT (n = 5) or *uxt1*Δ *uxt2*Δ (n = 10). Results shown are combined from two independent experiments. **, $p < 0.01$; ***, $p < 0.005$ by the log-rank test.

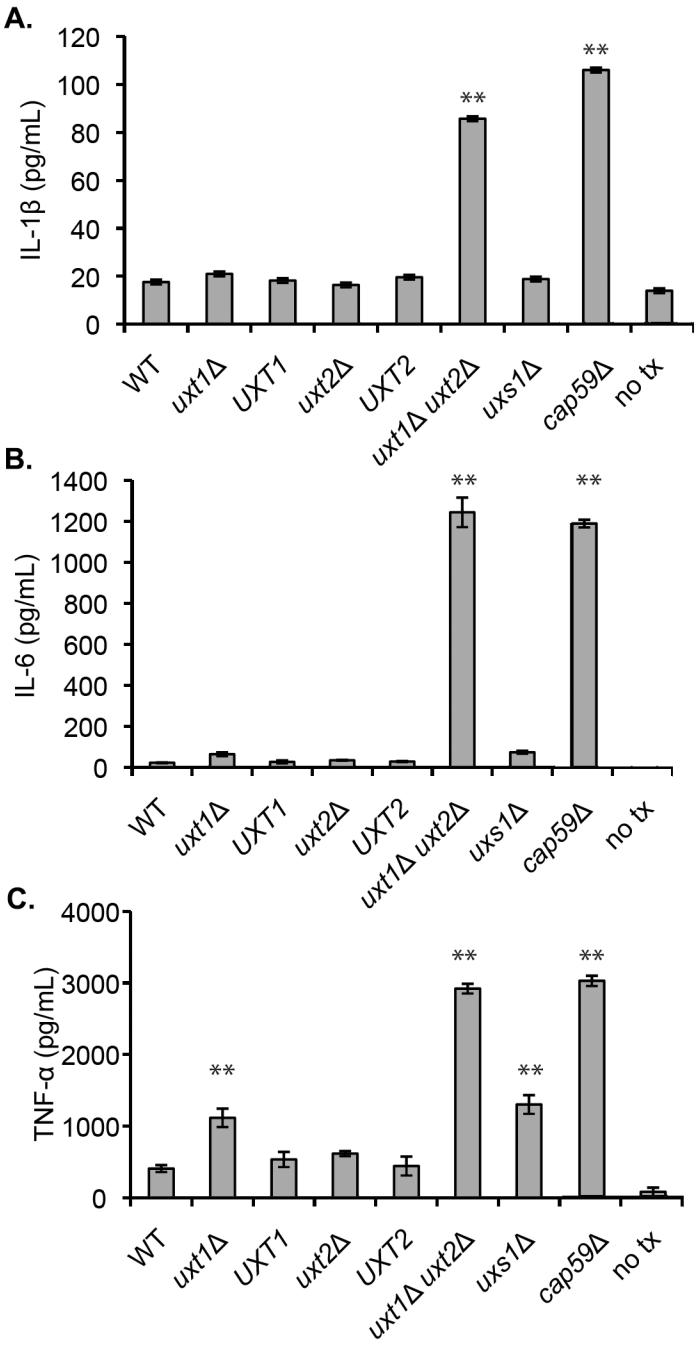

Figure 4. Cytokine production by dendritic cells stimulated with cryptococcal antigens. DCs were co-incubated for 24 h with heat-killed cells of the strains indicated or subjected to no treatment (no tx). Levels of (B) IL-1β, (C) IL-6, and (D) TNF-α in the supernatant were quantified by ELISA. Data shown is the mean ± SD (n = 3) of one representative experiment from five independent experiments that yielded similar results. **, $p < 0.01$ by one-way ANOVA with Tukey's post hoc test.

SUPPLEMENTARY MATERIAL

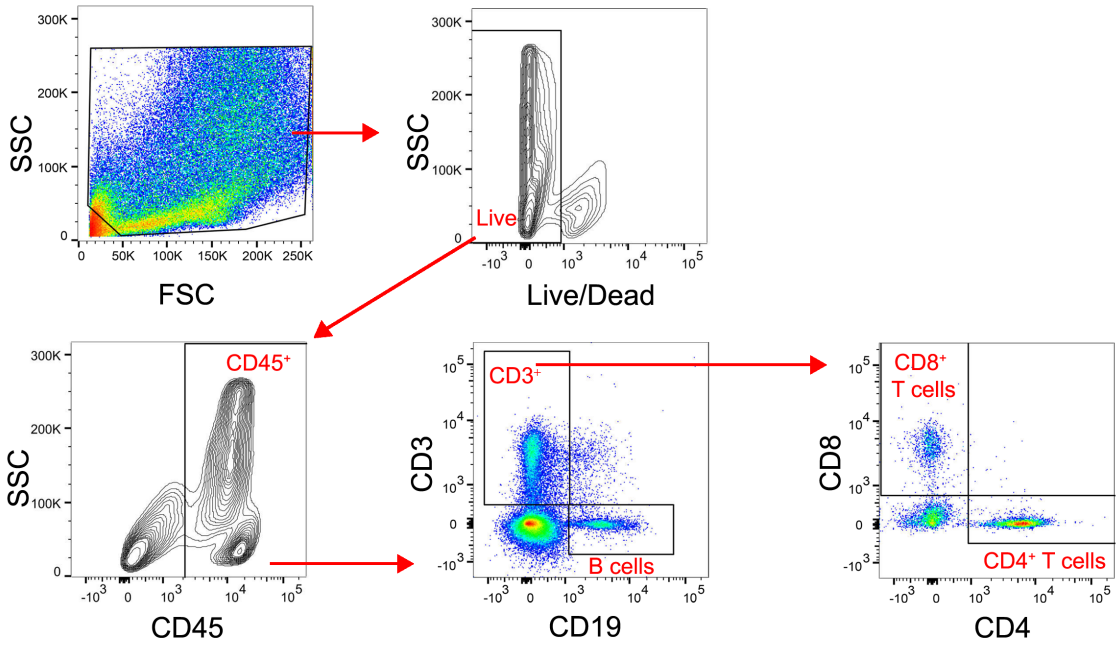

Supplemental Figure 1. Example of the multi-color flow cytometry gating strategy used to enumerate lung infiltrating immune cells.

Table S1. *C. neoformans* strains utilized in these studies.

C. neoformans strain[a]	Origin
KN99α	(Nielsen et al., 2003)
*uxt1*Δ	(Li et al., 2018)
UXT1	(Li et al., 2018)
*uxt2*Δ	(Li et al., 2018)
UXT2	(Li et al., 2018)
*uxt1*Δ *uxt2*Δ	(Li et al., 2018)
*uxs1*Δ	(Gish et al., 2016)
*cap59*Δ	(Moyrand and Janbon, 2004)

[a] All mutant strains are derived from KN99α

Table S2. Antibodies for flow analysis.

Antigen	Clone	Fluorophore	Dilution	Company	RRID
CD3	17-A2	APC-Cy7	1:250	BioLegend	AB_2242784
CD4	GK1.5	BUV737	1:500	BD Biosciences	AB_2738734
CD8a	53-6.7	BV650	1:125	BD Biosciences	AB_2738084
CD16/CD32 Fc Block	2.4G2	(not applicable)	1:500	BD Biosciences	AB_394656
CD19	1D3	BV786	1:125	BD Biosciences	AB_2738141
CD45	30-F11	Pacific Blue	1:250	BioLegend	AB_493535

REFERENCES FOR SUPPLEMENTAL MATERIAL

Gish, S.R., Maier, E.J., Haynes, B.C., Santiago-Tirado, F.H., Srikanta, D.L., Ma, C.Z., Li, L.X., Williams, M., Crouch, E.C., Khader, S.A.*, et al.* (2016). Computational analysis reveals a key regulator of Cryptococcal virulence and determinant of host response. mBio *7*, e00313-00316.

Li, L.X., Rautengarten, C., Heazlewood, J.L., and Doering, T.L. (2018). Xylose donor transport is critical for fungal virulence. PLoS Pathog *14*, e1006765.

Moyrand, F., and Janbon, G. (2004). UGD1, encoding the *Cryptococcus neoformans* UDP-glucose dehydrogenase, is essential for growth at 37 degrees C and for capsule biosynthesis. Eukaryot Cell *3*, 1601-1608.

Nielsen, K., Cox, G.M., Wang, P., Toffaletti, D.L., Perfect, J.R., and Heitman, J. (2003). Sexual cycle of *Cryptococcus neoformans var. grubii* and virulence of congenic a and alpha isolates. Infection and immunity *71*, 4831-4841.